X-755-74-210
PREPRINT
NASA TM X- 70695

FLUORESCENCE AND PHOSPHORESCENCE OF PHOTOMULTIPLIER WINDOW MATERIALS UNDER ELECTRON IRRADIATION

W. VIEHMANN
A. G. EUBANKS
J. H. BREDEKAMP

JULY 1974

GSFC — GODDARD SPACE FLIGHT CENTER —
GREENBELT, MARYLAND

FLUORESCENCE AND PHOSPHORESCENCE OF PHOTOMULTIPLIER WINDOW MATERIALS UNDER ELECTRON IRRADIATION

W. Viehmann

A. G. Eubanks

and

J. H. Bredekamp

GODDARD SPACE FLIGHT CENTER
Greenbelt, Maryland

FLUORESCENCE AND PHOSPHORESCENCE OF PHOTOMULTIPLIER WINDOW MATERIALS UNDER ELECTRON IRRADIATION

W. Viehmann, A. G. Eubanks and J. H. Bredekamp

ABSTRACT

The fluorescence and phosphorescence of photomultiplier window materials under electron irradiation have been investigated using a Sr^{90} - Y^{90} beta-emitter as the electron source. Spectral emission curves of uv-grade, optical-grade and electron-irradiated samples of MgF_2 and LiF, and of CaF_2, BaF_2, Sapphire, Fused Silica, and uv-transmitting glasses were obtained over the spectral range of 200 nm to 650 nm. Fluorescence yields, expressed as the number of counts in a solid angle of 2π steradian per 1 MeV of incident electron energy deposited (MeV^{-1} $(2\pi\ ster)^{-1}$), were determined on these materials utilizing photomultiplier tubes with cesium telluride, bialkali, and trialkali (S-20) photocathodes, respectively. Typical yields observed with a uv/visible sensitive bialkali cathode range from 10 MeV^{-1} $(2\pi\ ster)^{-1}$ for uv-grade MgF_2 to $\simeq$200 MeV^{-1} $(2\pi\ ster)^{-1}$ for CaF_2. For comparison, sodium-activated cesium iodide, one of the most efficient scintillator materials, yields about 700 MeV^{-1} $(2\pi\ ster)^{-1}$. High-purity fused silica has the lowest yield, approximately 6 MeV^{-1} $(2\pi\ ster)^{-1}$. Optical-grade MgF_2 and LiF, as well as electron-irradiated uv-grade samples of these two materials show enhanced fluorescence due to color-center formation and

associated emission bands in the blue and red wavelength regions. Large variations in fluorescence intensities were found in uv-grade sapphire samples of different origins, particularly in the red end of the spectrum, presumably due to various amounts of chromium-ion content. Phosphorescence decay with time is best described by a sum of exponential terms, with time constants ranging from a few minutes to several days.

Phosphorescence intensity expressed as a fraction of the steady-state fluorescence intensity is an extremely sensitive measure of crystalline perfection and purity. This fraction ranges from a high of $\simeq 10^{-2}$ for some fluoride samples to a low of $\leqslant 2 \times 10^{-6}$ for fused silica. Application of the parameters obtained in this work to the analysis of recent flight observations on low light-level experiments yield good quantitative agreement with flight data from OAO-3 and OSO-7.

I. INTRODUCTION

Low light-level experiments and sensors carried on spacecraft and operating in the ultraviolet and visible regions at count rates, $\dot{N}$, of $10^2 \leqslant \dot{N} \leqslant 10^6$ counts per second have shown saturation* while passing through the South-Atlantic Anomaly (SAA) and considerably enhanced dark count rates for long periods of time after passage through the SAA. The South-Atlantic Anomaly is a region of increased, altitude dependent, electron and proton fluxes with fluxes ranging for electrons up to $>10^6$ cm^{-2} sec^{-1} and for protons up to $>10^4$ cm^{-2} sec^{-1}.[1] Well over 90% of the electrons have energies less than 2 MeV and most of the protons have energies less than 5 MeV. However, the tails of the energy distributions extend to >4 MeV for electrons and >100 MeV for protons, respectively. On OSO-7, for example, the Star Scanner, which utilizes a photomultiplier tube having a trialkali (E-type or ~S-20) photocathode and a Corning glass 7056 faceplate, and normally operates at signal count rates of approximately 2×10^5 sec^{-1}, goes into saturation; i.e., the rate increases to $>5 \times 10^5$ sec^{-1} while going through the region of maximum particle flux.[2] Because of the relatively high signal count rates and the high thermal dark counts associated with trialkali cathodes, however, enhanced dark count rates after passage through the SAA do not seem to be a problem in this case. On the OAO-3 (Copernicus) Princeton Experimental Package (PEP), on the other hand, in addition to saturation,

*"saturation" means that the count rate exceeds the dynamic range of the pulse counting electronics.

anomalously high dark count rates of the order of 200 to 300 sec^{-1} were encountered on uv/visible photomultipliers with bialkali (N-type) cathodes and MgF_2 windows for long periods after passing through the SAA.[3] It was also noted that dark count rates slowly diminished with time. Because of the low signal count rates of this experiment, ($\simeq 10^2$ sec^{-1}) and low thermal dark counts, these effects seriously compromise photometric accuracy if not taken into account.

It is thought that fluorescence of the photomultiplier window materials under energetic particle irradiation and subsequent slow decay (phosphorescence) are responsible for saturation and time-dependent dark counts, respectively.

In the present publication, we report our results of fluorescence and phosphorescence measurements on various photomultiplier window materials under electron irradiation from a Sr^{90}-Y^{90} beta source. Based on these results, we present our interpretation of flight observations together with recommendations for proper selection of window materials and shielding requirements for critical low light level experiments in space flight applications.

II. EXPERIMENTS

Objective

In order to characterize the luminescence properties of optical window materials under electron irradiation, the laboratory experiments were designed (1) to obtain the spectral distribution of fluorescence emission under steady-state condition, i.e., while the sample is being irradiated; (2) to measure the

fluorescence efficiency, or yield, i.e., the number of photons emitted, over a spectral interval of interest, per unit energy loss per electron; and (3) to measure the long-term time decay of phosphorescence after irradiation.

Materials

Table I lists window materials commonly used on vacuum-uv, uv, and visible photomultiplier tubes. The values given for the short-wavelength cut-off and 50% transmission points, respectively, are representative of the highest quality commercial materials available today. It is well known that these parameters are sensitive to purity and crystalline perfection of the materials. Therefore, we have included in our investigation samples of the materials listed in Table I of highest purity and perfection (uv-grade) as well as "optical-grade" samples of various materials, as far as they were available, in order to demonstrate the effect of material quality on the fluorescence and phosphorescence properties in question. In addition, uv-grade samples of MgF_2 and LiF were irradiated with 1-MeV electrons at fluences of up to 2×10^{13} $e^- cm^{-2}$ in order to study the effects of radiation damage on intensity and spectral distribution of optical emission.

Apparatus and Procedure

Electron Source

A 0.8 millicurie* $Sr^{90} - Y^{90}$ beta emitter having a circular active area of 0.28 cm^2 was used as the electron source. The maximum beta energies are

*1 Curie = 3.7×10^{10} disintegrations sec^{-1}.

0.544 MeV and 2.23 MeV, respectively, for Sr^{90} and Y^{90}, and the average beta energies are 0.194 MeV and 0.92 MeV, respectively. The composite beta spectrum for the Sr^{90}-Y^{90} equilibrium mixture is shown in Figure 1.

Measurements

In order to cover a wide spectral range, three photomultiplier tubes with different spectral response curves, as shown in Figure 2, were used. They were operated in the photon-counting mode in conjunction with a SSR-Model 1105 Photon Counter. For steady-state measurements the beta source was placed directly onto the sample to be measured at a fixed distance from the photomultiplier tube, as schematically shown in Figure 3. Spectral intervals were defined by the use of various cut-on filters, such as fused silica (λ 50% = 200 nm), Corning glass filter 9-54 (240 nm), Corning 7056 glass (310 nm), Lucite (350 nm), and a series of multi-layer interference filters ranging from 400 nm to 650 nm in 50 nm intervals. Background counts due to high-energy betas passing through the sample and filters, and/or due to fluorescence from the filter, were determined by placing a 50 μm thick (13.5 mg cm^{-2}) aluminum foil beneath the sample and filter, as also shown in Figure 3. The solid angle between sample and photomultiplier was kept well below 1.5 ster (80-degree cone), i.e., much smaller than the solid angle determined by total internal reflection at the faces of the disc-shaped samples.

III. RESULTS AND DISCUSSION

Emission Spectra

Luminescence spectra obtained on uv-grade, optical-grade, and electron-irradiated samples of MgF_2 are portrayed in Figure 4. Emission bands centered at ~225 nm, ~430 nm and ~600 nm can be discerned in all samples, with the position of the latter two bands being in good agreement with those observed by others on electron and gamma-irradiated MgF_2 under uv-excitation.[4] These emission bands arise from color centers or lattice defects inherent in the crystal or created by electron or gamma irradiation. As expected, these bands are weakest in unirradiated uv-grade material, stronger in optical-grade material and noticably enhanced after prolonged electron irradiation.

Lithium fluoride (Fig. 5) also emits over the whole spectral region, from its uv cut-off to the long wavelength limit of our experimental set-up (~650 nm). Emission bands can be distinguished at approximately 250 nm, 375 nm and 560 nm, respectively. Electron irradiation enhances both the blue and the orange emission bands, but depresses the uv emission by self-absorption in the 250 nm absorption band resulting from electron irradiation. (See insert in Fig. 5)

Oxygen ions substituting for fluorine ions in the crystal lattice are the most common and most difficult to eliminate "impurity" in fluorides. To illustrate the effect of such substitution, we have included in Figure 5 the emission and transmission spectra of an intentionally oxygen-doped LiF sample. The drastic

effect of oxygen substitution and of the lattice defect structure resulting from this substitution on the fluorescence spectrum and intensity and on transmission can be clearly seen.

Emission spectra of fused silica (SiO_2) sapphire (Al_2O_3), calcium fluoride (CaF_2), and barium fluoride (BaF_2) are shown in Figure 6. Overall, the emission intensities of CaF_2 and BaF_2 are considerably higher than those of MgF_2 and LiF and little difference was found between samples of different origin and of presumably different quality in terms of purity and perfection. Considerable variation was, however, encountered in the phosphorescence properties, as will be shown later. Similarly, sapphire samples showed little variation in the short-wavelength portion of the spectrum, but considerable differences were noted in the intensities of the long-wavelength peak partially shown in Figure 6. We attribute this red peak to chromium ions, the dopant intentionally used in Ruby (= $Al_2O_3 : Cr^{3+}$), which causes intense fluorescence centered at 690 nm. As an impurity, chromium is difficult to eliminate in aluminum oxide.

The emission intensities of fused silica and uv-transmitting glasses are quite weak and little, if any, differences were noted in total intensity and in spectral distribution between different samples of each material.

Luminescence Efficiency

Luminescence efficiency, ϵ, under charged particle excitation is defined as the ratio of specific luminescence, dL/dx, and specific energy loss of the particle, dE/dx, i.e.,

$$\epsilon = \frac{dL}{dE}. \qquad (1)$$

For most phosphors, this (differential) efficiency is a function of the specific energy loss, and has a rather flat maximum at 1 MeV cm^2g^{-1} $< dE/dx <$ 100 MeV cm^2g^{-1}.[5] For the average energy of Sr^{90}-Y^{90} betas (= 0.25 MeV), the specific energy loss of electrons in the materials investigated here is of the order of 2 MeV cm^2g^{-1}, i.e., in a range where dL/dE varies only little with energy. For practical purposes, therefore, we assume dL/dE to be constant over the energy range of Sr^{90}-Y^{90} betas and define our luminescence efficiency as

$$\epsilon = \frac{\Delta L}{N_{inc}\, E_{av}} \quad , \tag{2}$$

where N_{inc} is the number of electrons incident on the sample and E_{av} is the average energy per electron absorbed in the sample. If the sample thickness, t, is larger than the range, r (E_{max}), of electrons of maximum beta energy, E_{max}, all betas are absorbed and the average energy absorbed in the sample is equal to the average beta energy:

$$E_{av} = \frac{\int_0^{E_{max}} E\, N(E)\, dE}{\int_0^{E_{max}} N(E)\, dE} \quad , \tag{3}$$

where the beta energy distribution is normalized to unity per unit time, or

$$\int_0^{E_{max}} N(E)\, dE = 1 \quad .$$

For samples of thickness less than r (E_{max}) and an isotropically emitting beta source, the variation of the electron path length, ℓ, with angle of incidence, θ, has to be taken into account; i.e., the fraction of electrons which lose less

than their total energy has to be considered. This fraction is contained in a circular cone of half-angle θ_0, where θ_0 is the angle of incidence for which $\ell = t/\cos\theta_0$ is equal to the electron range, r (E_{max}). For the energy interval, between E and E + dE this fraction is given by $\Omega/2\pi = 1 - \cos\theta(E) = 1 - t/r(E)$, where Ω is the solid angle of the cone.

The average energy loss of betas with the distribution function N(E) then becomes:

$$E_{av} = \frac{\int_0^{E_{max}} E\,N(E)\,dE - \int_{E(r=t)}^{E_{max}} E\left(1 - \frac{t}{r(E)}\right)N(E)dE}{\int_0^{E_{max}} N(E)\,dE} \quad . \tag{3a}$$

Using energy-range tables for sapphire[6] and LiF[7] and assuming that variations of electron ranges expressed in mass per unit area (g cm^{-2}) for the materials investigated here are insignificant within the overall accuracy of our experiment, we have computed the average energy losses for Sr^{90}-Y^{90} betas for the individual sample thicknesses and calculated the luminescence efficiences according to Equation (2). In so doing, we have further assumed that the optical emission is isotropic, i.e., spherically symmetrical*. Futhermore, in addition to geometrical factors, the total light collected depends, of course, on the spectral

*The validity of this assumption was verified by tilting samples to angles up to 70° with no noticeable effect on observed count rate.

response curve of the photomultiplier tube and its overlap with the spectral emission of the various materials. It is impractical, therefore, to express ΔL as a singular, normalized quantity. For this reason, we have expressed the luminescence efficiency in units of counts in a solid angle of 2π ster per MeV of absorbed electron energy and present the results in Table II for three different photocathodes, namely a "solar-blind" CsTe cathode, a uv/visible sensitive bialkali cathode and a red-sensitive trialkali (S-20) photocathode, respectively. Their response curves were given in Figure 2. Also, for the sake of completeness, we have converted these efficiencies into units of photons per 100 nm per MeV, averaged over the bandpass of the respective photocathodes and over 4π steradians.

In order to get a reasonable estimate of the degree of validity of the various assumptions entering into the determination of efficiency values, we have included in Table II the results of measurements performed on a plastic scintillator material, on "undoped" cesium iodide, on sodium-activated CsI, and on thallium-activated CsI. The scintillation properties of those materials have been studied extensively[5] and their "absolute" efficiencies, defined as $\epsilon_{abs} = \frac{\text{total emitted energy}}{\text{total absorbed energy}}$ seem to be fairly well established.[5,8] In the practice of scintillation counting, "absolute" efficiencies of scintillator materials are determined by measuring their light-output with a S-11 photocathode relative to that of a "standard" crystal of

thallium-activiated sodium iodide for which an efficiency of 12 to 13 percent is the generally accepted value. NaI(Tl) emits in the blue, with a peak at ~410 nm, and meaningful efficiencies are obtained by this method for materials which emit in the same spectral region, such as CsI, CsI(Na) and Plastics. However, for materials whose peak emission occurs well outside of the S-11 response, efficiencies obtained with S-11 cathodes relative to that of NaI(Tl) are, although of practical importance, not very meaningful from a fundamental point of view. CsI(Tl), for instance, has its emission peak at ~560 nm, and only a fraction of the total emission is inside the S-11 response curve. Because of this spectral mismatch, "standard" efficiencies for CsI(Tl) are estimated to be about a factor of 2 to 2.5 lower than "true" efficiencies obtained with a better spectrally matched photocathode and/or proper convolution of spectral emission and spectral response curve of scintillator and photocathode, respectively.[9]

Based on our experimentally obtained count rates and on photocathode quantum efficiencies averaged over the spectral emission range of the various scintillator materials, we have computed "absolute" efficiency values for the four scintillators mentioned above and list the results in Table III, together with those given in the literature.[5,8] We observe reasonably good agreement for the blue-emitting materials but considerable discrepancy for CsI(Tl), as expected. Good agreement, however, is also obtained here, if "true" rather than "standard" absolute efficiencies are considered.

In examining Table II, we note again significant differences between uv-grade samples and optical-grade samples of MgF_2 and LiF, respectively, particularly in the long uv and visible wavelength regions. The growth of the blue and red emission bands with increasing electron dose is reflected in increased count rates obtained on irradiated samples with the bialkali and S-20 photocathodes, respectively. Small differences are noted between sapphire samples of different origin, and presumably different purity, in the short uv and uv/visible range, but considerable variations are noted with the red-sensitive S-20 photocathode, supposedly due to chromium impurities affecting the fluorescence peak near 700 nm, as mentioned previously. Calcium fluoride and barium fluoride were available only in optical-grade quality and very little difference was seen between samples of different origin. Note, however, the significantly higher luminescence yields over the entire spectral region in comparison to MgF_2 and LiF.

The luminescence yields of fused silica, uv-transmitting glasses, and borosilicate glass are comparable to those of uv-grade MgF_2 and LiF in the uv/visible region and significantly lower for red-sensitive cathodes, due to the relative weakness or absence of long-wavelength emission.

Time Decay of Phosphorescence

In all materials investigated here, with the exception of high-purity fused silica, slowly decaying phosphorescence was observed after removal of the beta excitation. Decay curves of various MgF_2 samples are presented in Figure 7

in double logarithmic representation. All decay curves, except where noted otherwise, were obtained after a 30-minute exposure to 0.4 mCi of SR^{90}-y^{90}. In good approximation, the time dependence of phosphorescence intensity can be described by a sum of exponential terms,

$$I_p(t) = \sum_i I_i \cdot \exp -\left(\frac{t - 1 \text{ min}}{\tau_i}\right) , \qquad (4)$$

where the time constants are characteristic of the material, and the absolute, as well as relative, values of the amplitudes, I_i, are a function of the purity, or quality, of the individual sample and of the total electron dose received by the sample. This is illustrated in Table IV, which lists the decay parameters (I_i, τ_i) for the various samples of PMT window materials, obtained by fitting their measured decay curves to decay functions of the form given in equation 4, with one set of time constants for each material. As a measure of the goodness of fit obtained under this premise, we list the RMS errors associated with the time constants, as well as a total error determined by the differences between the measured points of the decay curves and the fits. With a few exceptions, errors for the time constants are well below ten percent and total errors are generally less than twenty percent. Large errors are encountered in cases where decay rates are fast, or count rates are low, or both.

In examining Table IV, we note that for MgF_2 a minimum of three terms with time constants of 4.4 minutes, 200 minutes and 3600 minutes, respectively

is required to describe the phosphorescence decay adequately, and that considerable variations occur in the amplitude factors not only between optical grade and uv-grade material, but also among uv-grade samples themselves. It should be pointed out, however, that sample #2, exhibiting the most intense phosphorescence, represents uv-grade quality as it was available about six to seven years ago; whereas, the other MgF_2 samples were acquired recently. Thus, the considerable improvement in material quality over this period of time is illustrated by comparing the phosphorescence intensities of these two classes of material.

Shorter periods of beta excitation (sample #2a) result in lower amplitudes of the long time constant terms, whereas prolonged, intensive electron bombardment (sample #6) leads to overall enhancement of phosphorescence intensity, particularly of the long time constant component.

Typical decay curves of various other window materials are shown in Figure 8. LiF sample #1, representing uv quality material acquired about six years ago, was monitored over a period of 200 hrs, thus allowing the determination of four time constants of approximately 5 minutes, 20 minutes, 12 hrs and 93 hrs, respectively (see Table IV). The improvement of material quality and perfection achieved over the past years is also readily apparent by comparing present-day optical-grade (LiF #2) and uv-grade (LiF #3) with sample #1. Calcium fluoride and barium fluoride show more intense phosphorescence than MgF_2 and LiF, as

one might expect on the basis of their higher fluorescence yield. At least three time constants govern their phosphorescence decay. They are approximately 2 minutes, 44 minutes and 580 minutes for BaF_2 and 2.6 minutes, 14 minutes and 150 minutes for CaF_2.

All five samples of sapphire listed in Table IV are of uv quality and the wide range of phosphorescence intensity, comprising a factor of almost 10^3, is striking, particularly in view of the fact that the differentiation in luminescence yield is not nearly as pronounced (see Table II). This observation applies equally well to the fluorides reported on above. It is obvious that electron-induced phosphorescence, or the lack of it, is a much more sensitive measure of crystalline perfection and purity than luminescence efficiency, optical density of color center absorption bands, or uv cut-off. To illustrate this quantitatively, we have tabulated, in Table V, the ratios of phosphorescence intensities at t = 1 minute to fluorescence intensities under steady-state electron excitation. These ratios range from a low of $< 2 \times 10^{-6}$ for high-purity fused silica to a high of $\geqslant 10^{-2}$ for optical-grade MgF_2 and BaF_2.

UV-transmitting glasses exhibit a suprisingly high ratio of 0.5×10^{-3} to 1×10^{-3}. Their time-decay of phosphorescence (Fig. 8) is characterized by a minimum of two exponential terms of about equal amplitude and time constants of approximately 4 minutes and 57 minutes.

Additional Observations

It is generally agreed that phosphorescence in crystalline materials is due to electrons and holes trapped at lattice defects, or trapping sites, and their release to emitting centers by thermal agitation. Although it is neither intended nor possible to identify the centers involved or to elucidate their phosphorescence kinetics within the scope of this investigation, we would like to include some preliminary observations which seemingly illustrate the role of trapping centers in the phosphorescence mechanisms. Thermoluminescence measurements over the temperature range of 25°C to 300°C, performed after $Sr^{90}-Y^{90}$ beta irradiation, reveal well defined glow peaks in most materials. Four in MgF_2, LiF, CaF_2, and BaF_2; two in sapphire; and two rather broad peaks in Corning 9741 and Corning 7056 glass. The glow-peak temperatures are characteristic of each material; however, the relative peak heights vary from sample to sample as well as with electron dose. In some fluoride samples broad-band uv excitation results in glow curves identical to those observed after beta irradiation. In others, fewer peaks are obtained after uv exposure than after beta exposure. In the latter, certain traps populated by beta irradiation are emptied by subsequent uv irradiation, i.e., phosphorescence induced by electrons is quenched by uv.

These examples must suffice here to hint at possible relationships between trap concentration and trap-depth on the one hand and intensity and time-decay of phosphorescence on the other. Quantitative details remain to be investigated.

Interpretation of Flight Observations

Based on peak flux densities and energy distributions for electrons and protons as given by Stassinopoulos[10] for OSO orbits, we have calculated peak count-rates for 2.5 cm diameter PMTs, using a luminescence efficiency of 10 MeV^{-1} $(2\pi \text{ ster})^{-1}$. Within the overall accuracy of these calculations the results are equally valid for 7056 glass faceplates and S-20 photocathodes, and bialkali cathodes on uv-grade MgF_2 or LiF of $\geq$1 mm thickness. The results are presented in Figure 9, which shows the count-rates due to electrons and due to protons as a function of effective shielding, expressed in millimeters of aluminum. Several simplifying assumptions have been made in these calculations: (1) we have considered normal incidence only, and (2) we have assumed that the effect of the aluminum shielding on the energy spectrum of the transmitted particle fluxes is approximated by a sharp cut-on at the energy for which the thickness of the shielding equals the range at that particular energy. The resulting over-estimate on transmitted flux is off-set somewhat by assuming an energy independent, specific energy loss in the faceplate material of 0.4 MeV per mm for electrons and 4 MeV per mm for protons, respectively.

For "moderate" shielding of $\leq$4 mm of aluminum, fluorescence induced count-rates are predominantly due to electrons and are of the order of $\geq 8 \times 10^5$ sec^{-1}, in good agreement with observations on the OSO-7 star scanner. Flight data on the saturation count-rate on the Copernicus PEP Experiment are not available for comparison. However, dark counts taken about 30 minutes

after passage through the SAA are known to be in the 150 to 350 sec^{-1} range. Turning to curves (1), (2), and (2a) of Figure 7, we extrapolate for $t \rightarrow 1$ min to a count-rate of 2×10^3 $sec^{-1} < \dot{N} < 8 \times 10^3$ sec^{-1}. Using a ratio of phosphorescence to fluorescence of $\leq 1 \times 10^{-2}$ for "optical-grade" MgF_2 from Table V, we obtain a saturation count-rate of 2×10^5 $sec^{-1} \leq \dot{N} \leq 8 \times 10^5$ sec^{-1}, in reasonable agreement with computed values for moderate shielding.

The effect of electrons decreases sharply with increasing shielding because of the rapid decrease of electron flux beyond 4 MeV. Above an effective shielding of ≥ 7 mm of aluminum, fluorescence count-rates are entirely due to protons and diminish only slowly with increasingly heavier shielding.

IV. SUMMARY AND CONCLUSIONS

Fluorescence and phosphorescence of "state-of-the-art" photomultiplier window materials under charged particle irradiation are of sufficient magnitude to seriously impair low light level satellite experiments and sensors operating in the uv and/or visible regions, both during and after passage through orbital regions of enhanced high-energy charged particle flux. Luminescence efficiencies and time constants of phosphorescence decay determined in the laboratory on uv-grade window materials in conjunction with uv/visible sensitive bialkali photocathodes and visible-trialkali cathodes account for count-rates of $\gtrsim 1 \times 10^6$ sec^{-1} in the South Atlantic Anomaly as well as anomalously high dark count-rates of 10^2 to 10^3 sec^{-1} for periods of hours after passage through the SAA, in good agreement with recent flight observations.

Analysis indicates that shielding of PMT faceplates against electrons of energies up to 4 MeV will effectively reduce these count rates by about a factor of 10, the residual rates then being due to high energy protons of $E \geqslant 30$ MeV, for which shielding becomes impractical.

Laboratory measurements further indicate that substantial reduction of phosphorescence emission can be realized by careful selection of high-purity samples by means of a simple screening test based on the technique employed in this work.

Phosphorescence intensity is considerably more sensitive to crystalline perfection and purity than luminescence yield. It is highly probable, therefore, that proper shielding and material selection will lower phosphorescence induced dark count rates to acceptable levels. It remains doubtful, however, whether count rates in the high flux regions resulting from luminescence induced by high energy protons can be lowered to negligible levels.

Acknowledgments

The authors would like to express their gratitude to Dr. George F. Pieper for his continued interest and helpful discussions during the course of this work and to C. S. Sturgell, who supplied many of the samples and the Photomultipliers used in this work.

REFERENCES

1. E. G. Stassinopoulos, NASA SP 3054, (1970).

2. R. Gutshall, Ball Brothers Research Corp., private communication.

3. John B. Rogerson, Jr., Princeton University Observatory, private communication.

4. O. E. Facey and W. A. Sibley, Phys. Rev. B, Vol. 2, Nr 4, 1111, (1970).

5. J. B. Birks, "The Theory and Practice of Scintillation Counting," Pergamon Press, N. Y., (1964).

6. M. J. Berger and S. M. Selzer, "Energy Spectra and Angular Distribution of Electrons Transmitted Through Sapphire (Al_2O_3) Foils," NASA SP 3008, (1964).

7. M. J. Berger and S. M. Selzer, "Additional Stopping Power and Range Tables for Protons, Mesons and Electrons," NASA SP 3036 (1966).

8. G. F. J. Garlick, In "Luminescence of Inorganic Solids," Paul Goldberg, Editor, Academic Press, (1966), Chapter 12.

9. M. R. Farukhi, Harshaw Chem. Co., private communication.

10. E. G. Stassinopoulos, "The Radiation Environment of OSO Missions from 1974 to 1978," GSFC X-601-73-168, May 1973.

Table I

Photomultiplier Window Materials

Material	UV-Cutoff (nm) (10% Transmission)	50% Transmission Point (nm) 2 mm Thick
UV Grade LiF	105	122
UV Grade MgF_2	110	125
UV Grade CaF_2	110	126
UV Grade BaF_2	135	150
UV Grade Sapphire	145	160
Fused Silica	~160	~175
Corning 9741 Glass	200	230
Corning 7056 Glass	270	310

Table II

Luminiscence Efficiencies of PMT Window Materials and Some Scintillator Materials for UV, UV-Visible, and Visible Photocathodes

PMT	542F-08; $\eta_{av} = 0.06$ 100nm $< \lambda <$ 300nm		541N-09; $\eta_{av} = 0.15$ 130nm $< \lambda <$ 430nm		FW 130; $\eta_{av} = 0.18$ 320 $< \lambda <$ 570nm		Remarks
Material	cts/1 MeV	Photons/ 100nm, 1 MeV, 4π	cts/1 MeV	Photons/ 100nm, 1 MeV, 4π	cts/1 MeV	Photons/ 100nm, 1 MeV, 4π	
MgF_2							
UV Grade, Manufacturer A	0.8	13	8	36	32	142	
UV Grade, Manufacturer B	1.3	21	5	22	15	67	
UV Grade (A), irradiated $2 \times 10^{13} e^{-}cm^{-2}$ (1-MeV)	1.1	18	25	110	85	380	
Optical Grade	1.4	23	9	40	52	230	
UV-Grade	–	–	17	76	–	–	Faceplate of PMT
LiF							
UV Grade	2.5	42	10	44	9	40	
UV Grade, irradiated $5 \times 10^{12} e^{-}cm^{-2}$ (1-MeV)	2.2	37	14	62	22	98	
UV Grade, irradiated $>2 \times 10^{13} e^{-}cm^{-2}$ (1-MeV)	<2(a)	<35	17	75	25	110	
Optical Grade	1.7	28	10	45	19	85	
UV Grade	3	50	–	–	–	–	Faceplate of PMT
O_2 Doped	(a)		53	235	83	370	Intentionally doped with Oxygen

Table II (Continued)

PMT	542F-08; η_{av} = 0.06 100nm < λ < 300nm		541N-09; η_{av} = 0.15 130nm < λ < 430nm		FW 130; η_{av} = 0.18 320 < λ < 570nm		Remarks
Material	cts/1 MeV	Photons/ 100nm, 1 MeV, 4π	cts/1 MeV	Photons/ 100nm, 1 MeV, 4π	cts/1 MeV	Photons/ 100nm, 1 MeV, 4π	
CaF_2							
Optical Grade Manufacturer A	45	750	205	910	430	1900	
Optical Grade, Manufacturer B	41	680	200	890	350	1550	
Sample C	42	700	220	980	300	1330	Regrown by Czochralski Method from Optical Grade (B) Material
BaF_2							
Optical Grade, Manufacturer A	26	430	152	675	420	1870	
Optical Grade, Manufacturer B	26	430	170	755	440	1960	
Al_2O_3							
Sample #1	4	70	26	115	120	533	All samples are "UV Grade"
Sample #2	Not Measured		22	100	87	386	
Sample #3	3	50	19	85	26	115	
Sample #4	2	35	20	90	200	890	
Sample #5	3	50	20	90	28	125	

Table II (Continued)

PMT	542F-08; η_{av} = 0.06 100nm <λ<300nm		541N-09; η_{av} = 0.15 130nm <λ <430nm		FW 130; η_{av} = 0.18 320 <λ <570nm		Remarks
Material	cts/1 MeV	Photons/ 100nm, 1 MeV, 4π	cts/1 MeV	Photons/ 100nm, 1 MeV, 4π	cts/1 MeV	Photons/ 100nm, 1 MeV, 4π	
Spectrosil	1.2	20	6.5	29	9	40	
7940	1	17	6	27	8	35	
Suprasil	1	17	7	31	9	40	
8337 Glass	(a)		8	35	15	67	
9741 Glass	(a)		6	27	17	75	
7056 Glass	(a)		2(a)	9	8	35	
Plastic Scintillator	(a)		250	1120	360	1500	
CsI							
Undoped	(a)		170	755	240	1070	
Na-Activated	(a)		680	3020	2400	10,700	
Tl-Activated	(a)		825	3650	4200	18,700	

(a) Self-absorbing

Table III

Absolute Scintillation Efficiencies of CsI(Tl), CsI(Na), CsI, and Plastic Scintillator

Material	Absolute Scintillation Efficiency (%)		
	Present Work		Ref. 5, 8
	541N-09	S-20	S-11
CsI(Tl)	18	20	6 to 7
Cs(Na)	5.8	7.8	4.5
CsI	1.2	0.8	—
Plastic Scintillator	2	1	2

Table IV

Decay Parameters of Phosphorescence

$$I_p(t) = \sum_i I_i \exp -\left(\frac{t - 1\ \text{min}}{\tau_i}\right)$$

Material	Time Constants (min)	Sample #	Count Rate; $sec^{-1}(2\pi\ ster)^{-1}$ [a,b] I_1	I_2	I_3	I_4	RMS Error % τ_1	τ_2	τ_3	τ_4	Total	Remarks
MgF_2	τ_1 = 4.4	1	1.4×10^5	3.1×10^4	3×10^3	*	4.7	2.4	2.8	*	7.5	UV grade
		2	1.2×10^6	2.1×10^5	2×10^4	*	4.2	5.4	1.2	*	10	UV grade (old)
	τ_2 = 200	2a[c]	6.7×10^5	1.1×10^4	0	–	2.9	12.8	–	–	20	UV grade (old)
	τ_3 = 3600	3	4.9×10^5	5×10^4	0	–	5.6	2.5	–	–	12	Optical grade
		4	1.3×10^4	2.4×10^3	0	–	3	1.8	–	–	16	UV grade
		5	4.6×10^3	2.5×10^3	4.7×10^2	*	7	9.2	9.4	–	11	UV grade
		6	1.1×10^5	7.4×10^3	1.4×10^4	*	9	5.6	5.6	*	16	after $2 \times 10^{13} e^- cm^{-2}$ (1 MeV)
LiF	τ_1 = 4.6	1	2.1×10^5	6.9×10^5	3.5×10^4	8.2×10^3	8.7	1	7	2.7	9.5	UV grade (old)
	τ_2 = 20	2	1.8×10^4	9.6×10^4	3.4×10^3	*	7.6	1.5	1.8	*	6.3	Optical grade
	τ_3 = 740	3	1.8×10^4	1.5×10^4	4.6×10^2	*	3.5	1.6	4.5	*	15	UV grade
	τ_4 = 5600											
BaF_2	τ_1 = 2	1	6.3×10^6	2.8×10^6	8.3×10^4	*	2.8	1.4	5.4	*	7	Optical grade
	τ_2 = 45											
	τ_3 = 580											
CaF_2	τ_1 = 2.7	1	2.7×10^6	3.9×10^5	1.1×10^5	*	1	4	0.03	*	3	Optical grade
	τ_2 = 14											
	τ_3 = 150	2	8×10^3	2×10^5	1.5×10^5	*	25	3	0.4	*	3	
Al_2O_3	τ_1 = 1.8	1	2.6×10^5	5.3×10^3	5.3×10^2	0	4.5	20	3	*	23	
	τ_2 = 14	2	8×10^4	1.2×10^3	0	–	3	11	–	–	14	
	τ_3 = 227	3	2.8×10^3	1×10^2	0	–	1.7	10	–	–	8	UV grade
		4	4.6×10^2	1×10^2	5.2×10^1	0	3	9	0.05	–	8	
		5	1.3×10^2	2.3×10^1	0	–	2.5	2.5	–	–	30	
9741 glass	τ_1 = 4.2	1	6.5×10^3	2.6×10^3	0	–	5	2	–	–	7	as received
	τ_2 = 57	2	2.6×10^4	1×10^4	0	–	5	2	–	–	7	after $10^{14} e^- cm^{-2}$ (1 MeV)

a) N-09 Photocathode

b) After β-excitation of $9.5 \times 10^{10} cm^{-2}$ (0.25 MeV average energy)

c) Sample 2 after β-excitation of $9.5 \times 10^9 cm^{-2}$ (0.25 MeV)

*Not determined

0 Not significant within accuracy of measurement

Table V

$$\zeta = \frac{\text{Phosphorescence Intensity at } t = 1 \text{ min}}{\text{Fluorescence Intensity under steady state electron excitation}}$$

Material	ζ	Photomultiplier: 541 N-09
MgF_2		
UV Grade	0.250×10^{-3}	
	0.200×10^{-3}	
Optical Grade	10.000×10^{-3}	
	5.000×10^{-3}	
LiF		
UV Grade	1.000×10^{-3}	
Optical Grade	3.000×10^{-3}	
CaF_2		
	0.400×10^{-3} to 4.000×10^{-3}	
BaF_2	16.000×10^{-3}	
Sapphire		
#1	2.500×10^{-3}	
#2	not measured	
#3	0.050×10^{-3}	
#4	0.010×10^{-3}	
#5	0.005×10^{-3}	
Spectrosil	$<0.002 \times 10^{-3}$	
Suprasil	0.020×10^{-3}	
UV Glasses	0.500×10^{-3}	
	1.000×10^{-3}	

FIGURE CAPTIONS

Figure 1. Composite Beta Spectrum of Strontium^{90}-Yttrium^{90} Equilibrium Mixture

Figure 2. Spectral Response Curves of CsTe (542F), Bialkali (541N) and S-20 (FW 130) Photocathodes

Figure 3. Schematic Diagram of Measurement Setup

Figure 4. Spectral Emission Curves of Magnesium Fluoride Samples (1) UV-Grade; (2) Optical-Grade; (3) UV-Grade After Irradiation with 2×10^{11} $e^- cm^{-2}$ (1 MeV); (4) UV-Grade After Irradiation with 2×10^{13} $e^- cm^{-2}$ (1 MeV)

Figure 5. Spectral Emission Curves of Lithium Fluoride Samples (1) Optical-Grade; (2) UV-Grade After Irradiation with $\sim 10^{11}$ $e^- cm^{-2}$ (1 MeV); (3) UV-Grade After Irradiation with $\sim 5 \times 10^{12}$ $e^- cm^{-2}$ (1 MeV); (4) Oxygen-doped LiF. Insert: Spectral Transmissions of Samples (2), (3) and (4)

Figure 6. Emission Spectra of Calcium Fluoride, Barium Fluoride, Sapphire and Fused Silica

Figure 7. Phosphorescence Decay of Magnesium Fluoride After Exposure to 0.4 m $ClSr^{90}$-Y^{90} for 30 min. (9.5×10^{10} $e^- cm^{-2}$ of 0.25 MeV average energy)

(1), (4) and (5): Present-day UV-Grade MgF_2

(2): PMT-Faceplate, representative of "State-of-the-art" UV-grade MgF_2 of about 1968

(2a): Same as (2), except for shorter exposure time of 3 min.

(3): Present-day optical-grade

(6): UV-Grade, irradiated to 2×10^{13} $e^- cm^{-2}$ (1 MeV)

Figure 8. Typical Phosphorescence Decay Curves of BaF_2, CaF_2, LiF, Al_2O_3 and 9741 glass, after Exposure to 0.4 m Ci Sr^{90}-Y^{90} for 30 min. (9.5×10^{10} $e^- cm^{-2}$ of 0.25 MeV average energy)

Figure 9. Calculated electron and proton induced count-rates for peak flux densities of OSO orbits (550 km) as a function of effective shielding. Curves are representative of S-20 photocathodes on 2.5 cm dia/1 mm thick 7056 glass and bialkali cathodes on UV-grade MgF_2 or LiF of the same dimensions.

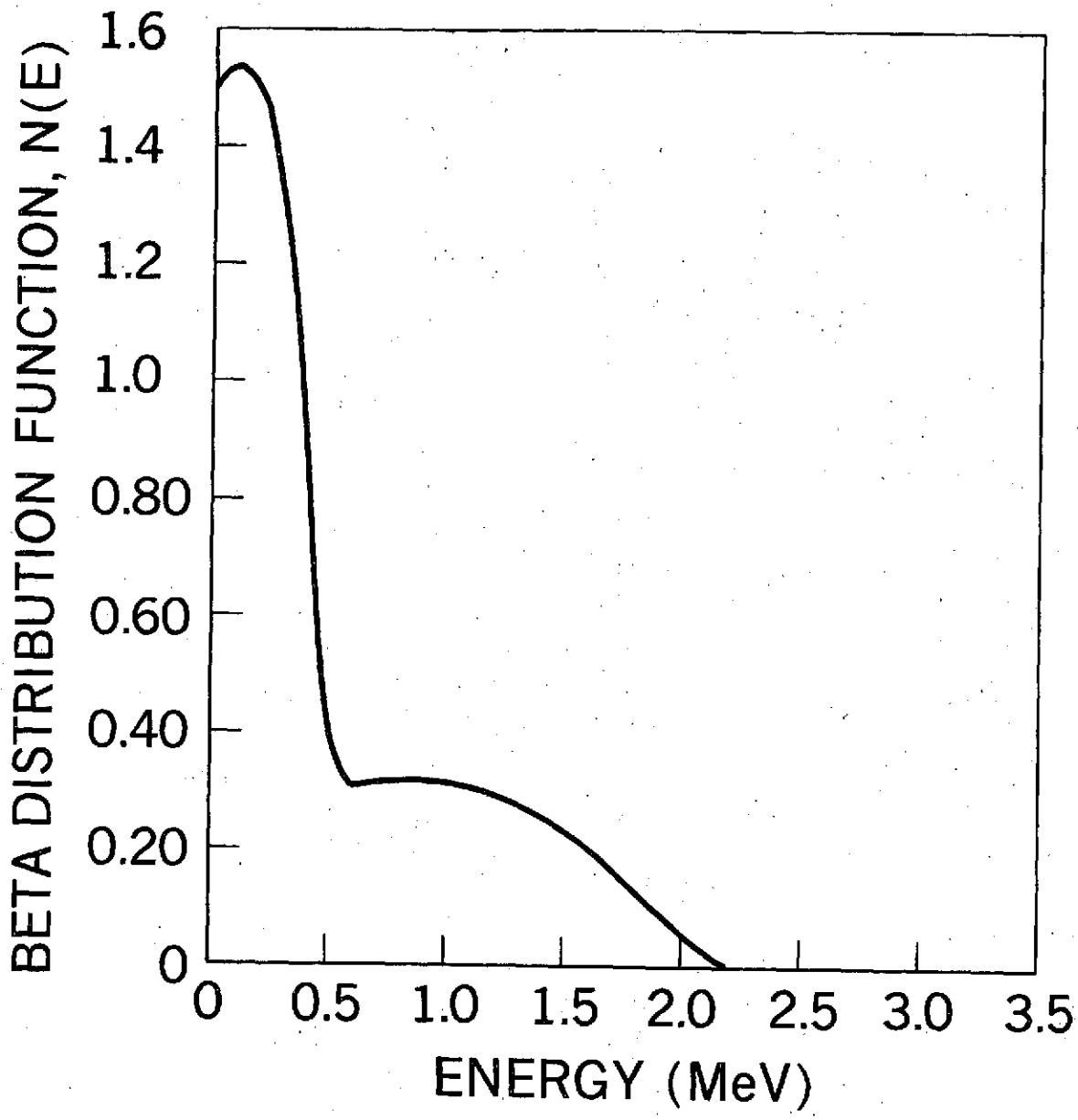
BETA DISTRIBUTION FUNCTION, N(E)
1.6
1.4
1.2
1.0
0.80
0.60
0.40
0.20
0
0
0.5
1.0
1.5
2.0
2.5
3.0
3.5
ENERGY (MeV)

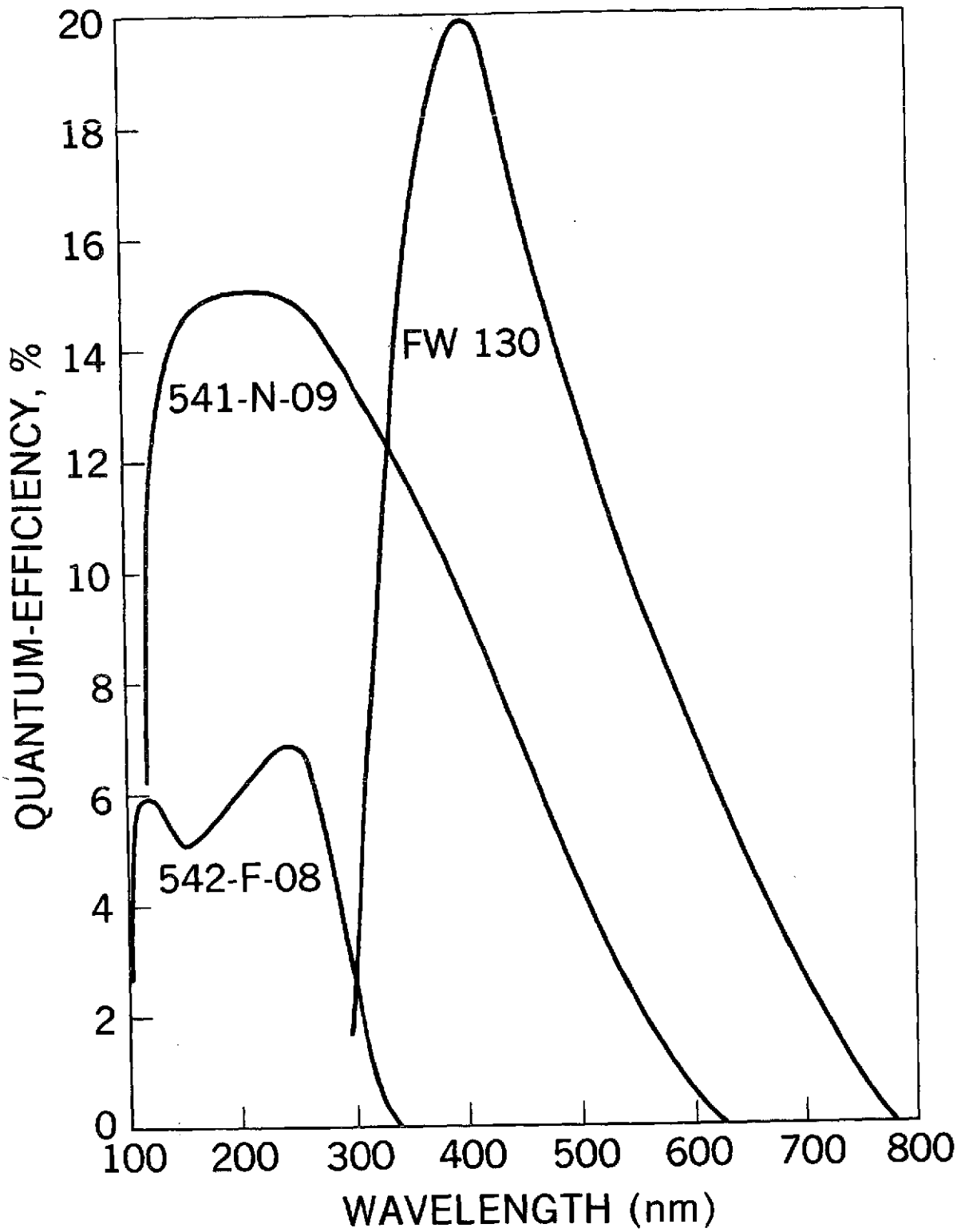
20
18
16
14
12
10
8
6
4
2
0
QUANTUM-EFFICIENCY, %
FW 130
541-N-09
542-F-08
100
200
300
400
500
600
700
800
WAVELENGTH (nm)

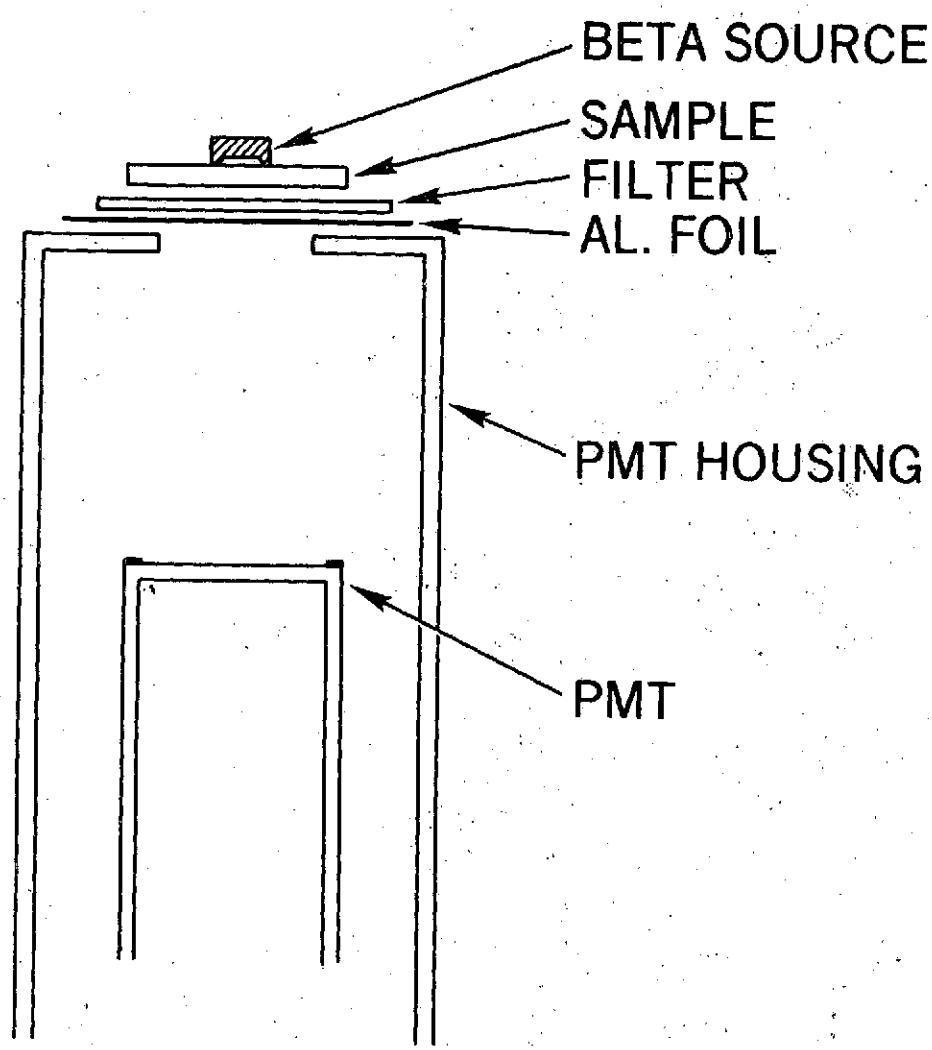
BETA SOURCE
SAMPLE
FILTER
AL. FOIL
PMT HOUSING
PMT

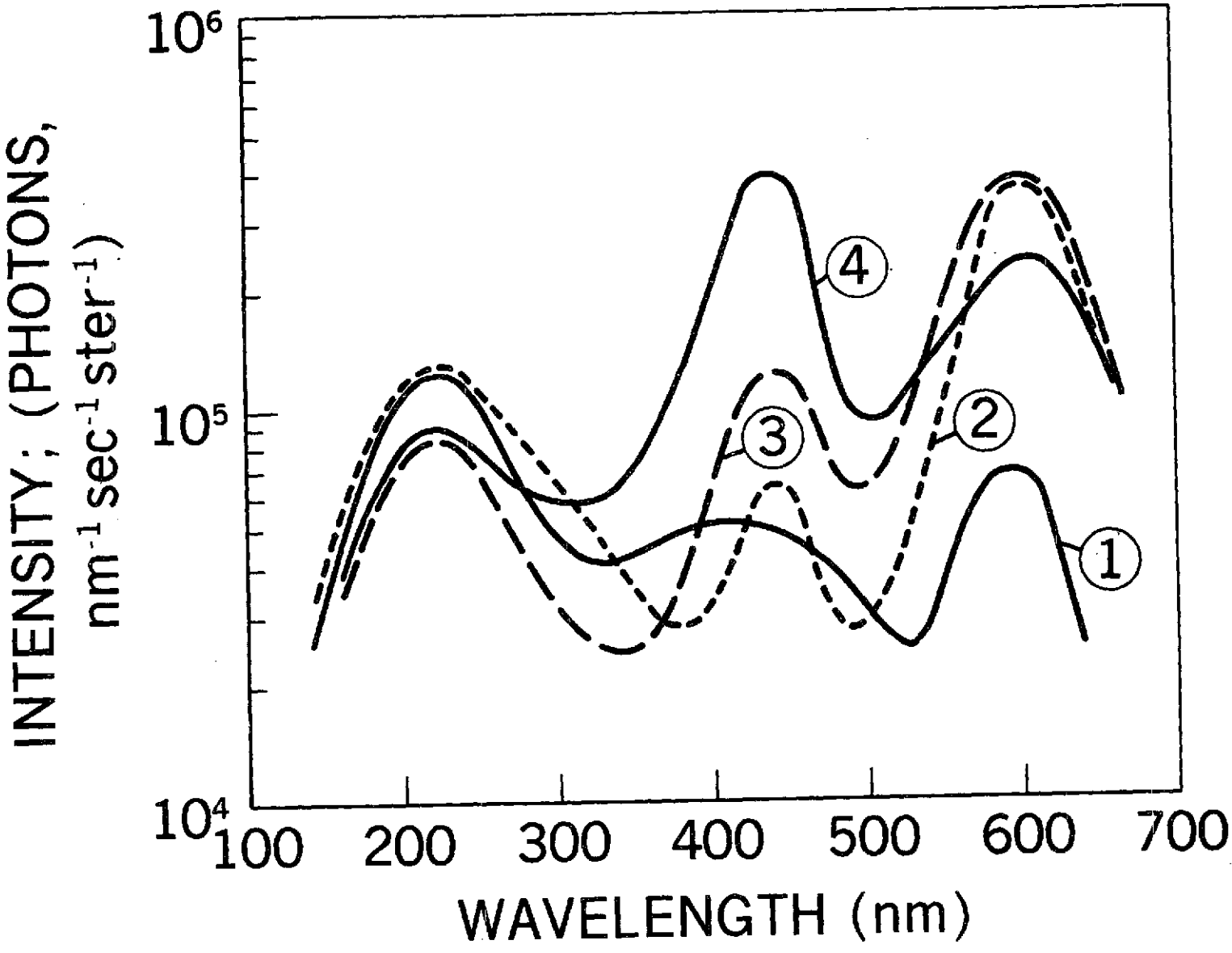
INTENSITY; (PHOTONS, nm⁻¹ sec⁻¹ ster⁻¹)
10⁶
10⁵
10⁴
100
200
300
400
500
600
700
WAVELENGTH (nm)
1
2
3
4

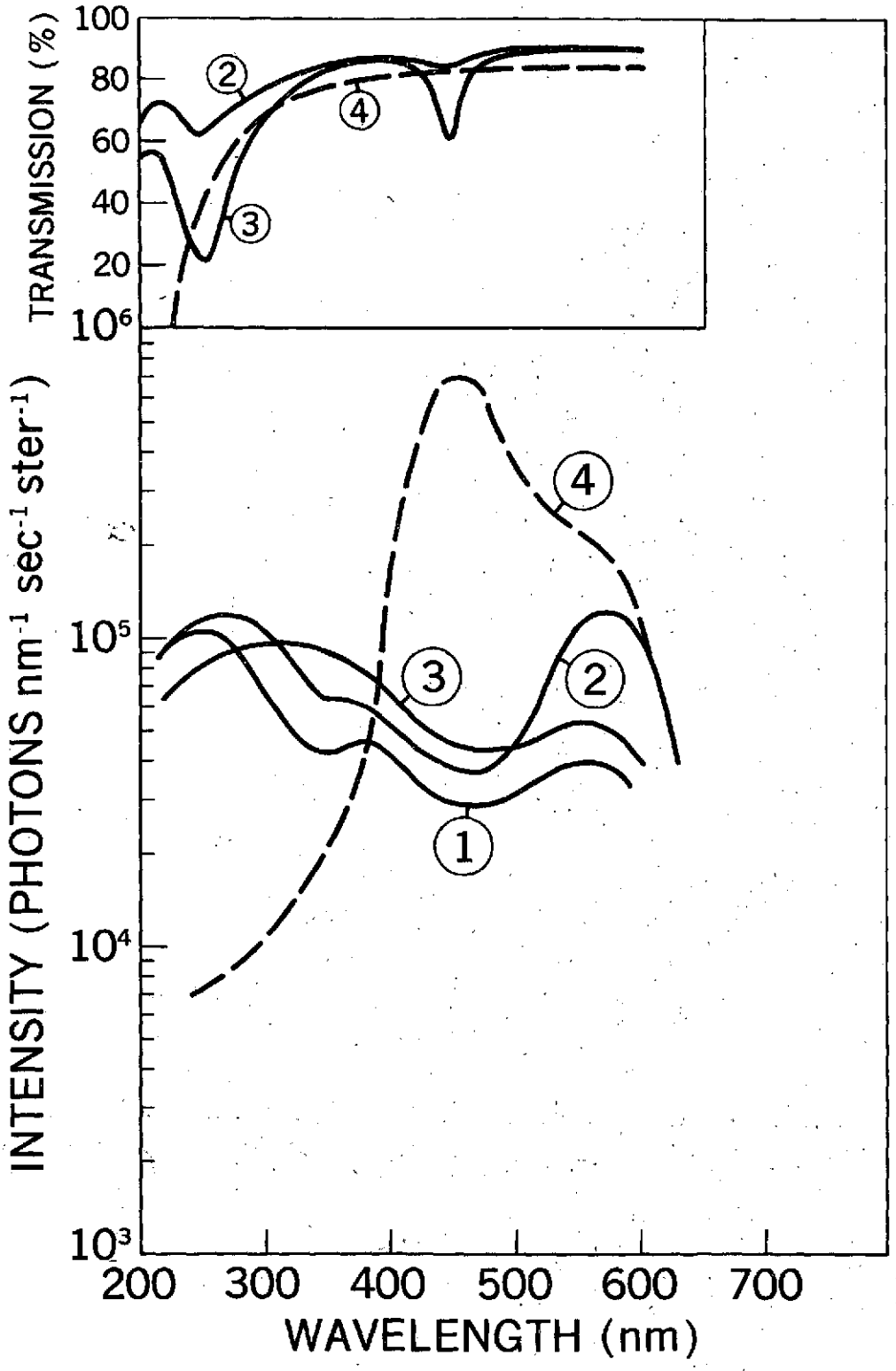
TRANSMISSION (%)
100
80
60
40
20
2
4
3
INTENSITY (PHOTONS nm⁻¹ sec⁻¹ ster⁻¹)
10⁶
10⁵
10⁴
10³
4
3
2
1
200
300
400
500
600
700
WAVELENGTH (nm)

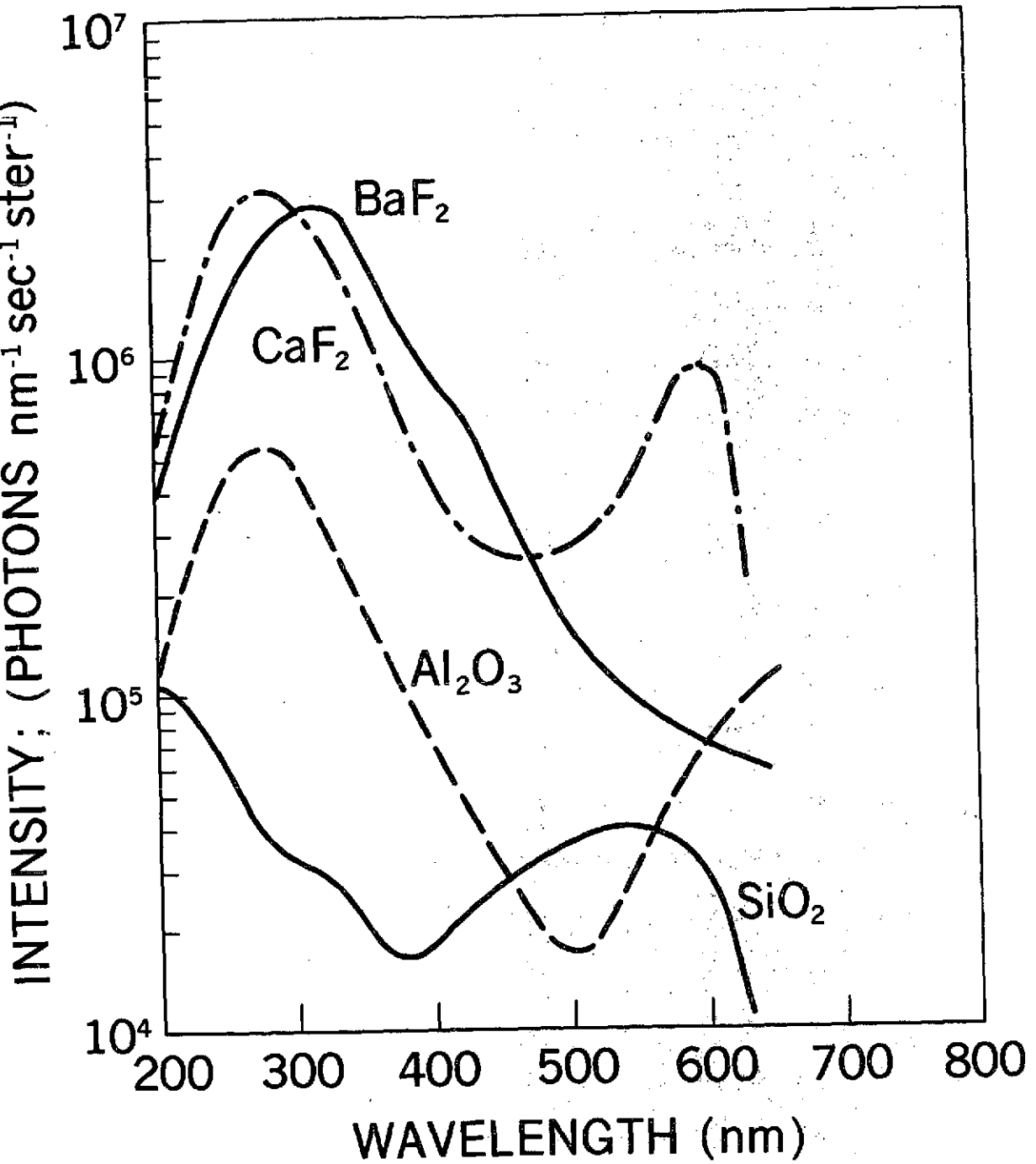
10^7
10^6
10^5
10^4
INTENSITY; (PHOTONS nm^{-1} sec^{-1} $ster^{-1}$)
BaF_2
CaF_2
Al_2O_3
SiO_2
200
300
400
500
600
700
800
WAVELENGTH (nm)

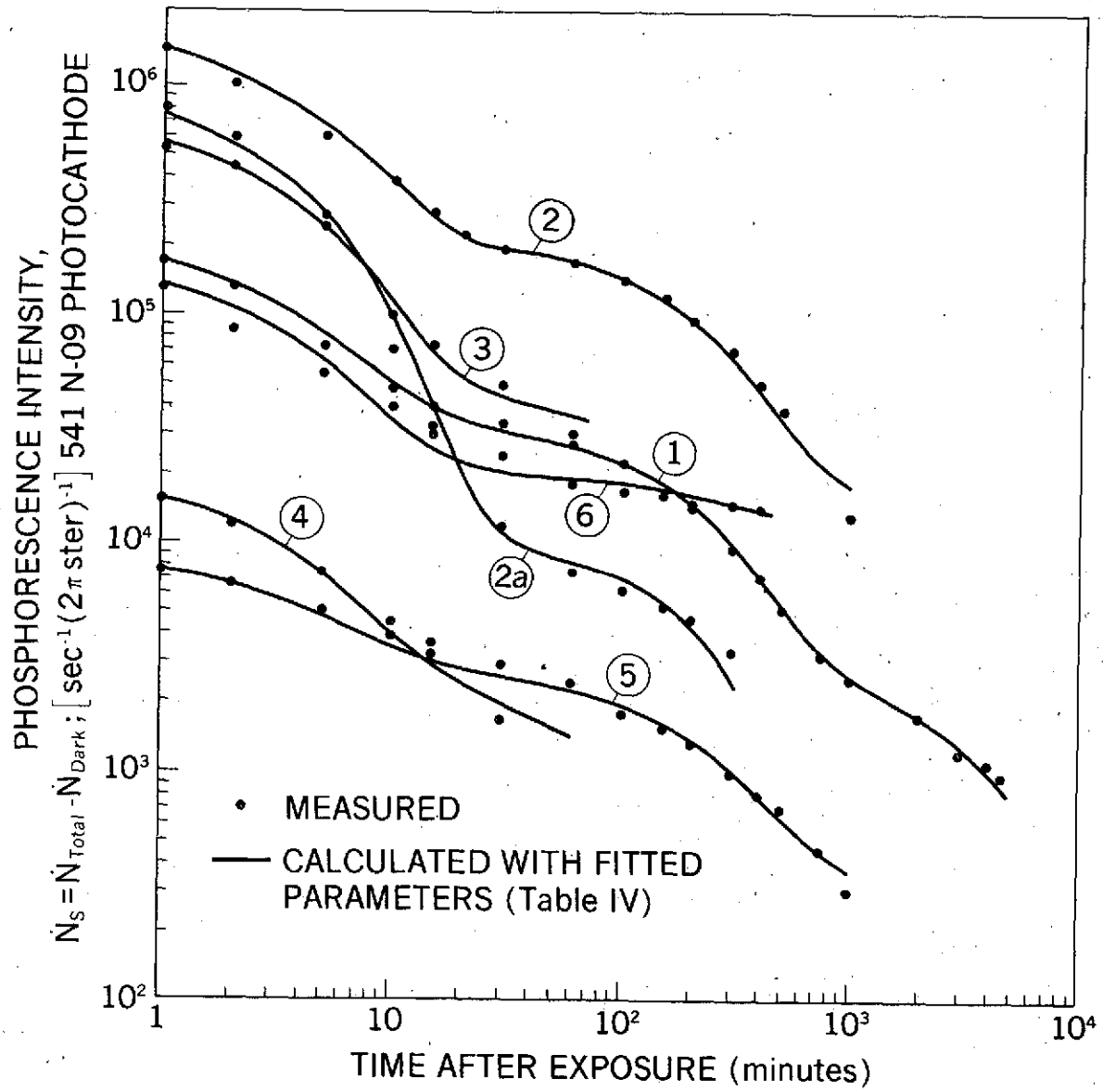
PHOSPHORESCENCE INTENSITY,
$\dot{N}_S = \dot{N}_{Total} - \dot{N}_{Dark}$; [sec^{-1} (2π ster)$^{-1}$] 541 N-09 PHOTOCATHODE
10^6
10^5
10^4
10^3
10^2
1
10
10^2
10^3
10^4
TIME AFTER EXPOSURE (minutes)
MEASURED
CALCULATED WITH FITTED PARAMETERS (Table IV)
1
2
2a
3
4
5
6

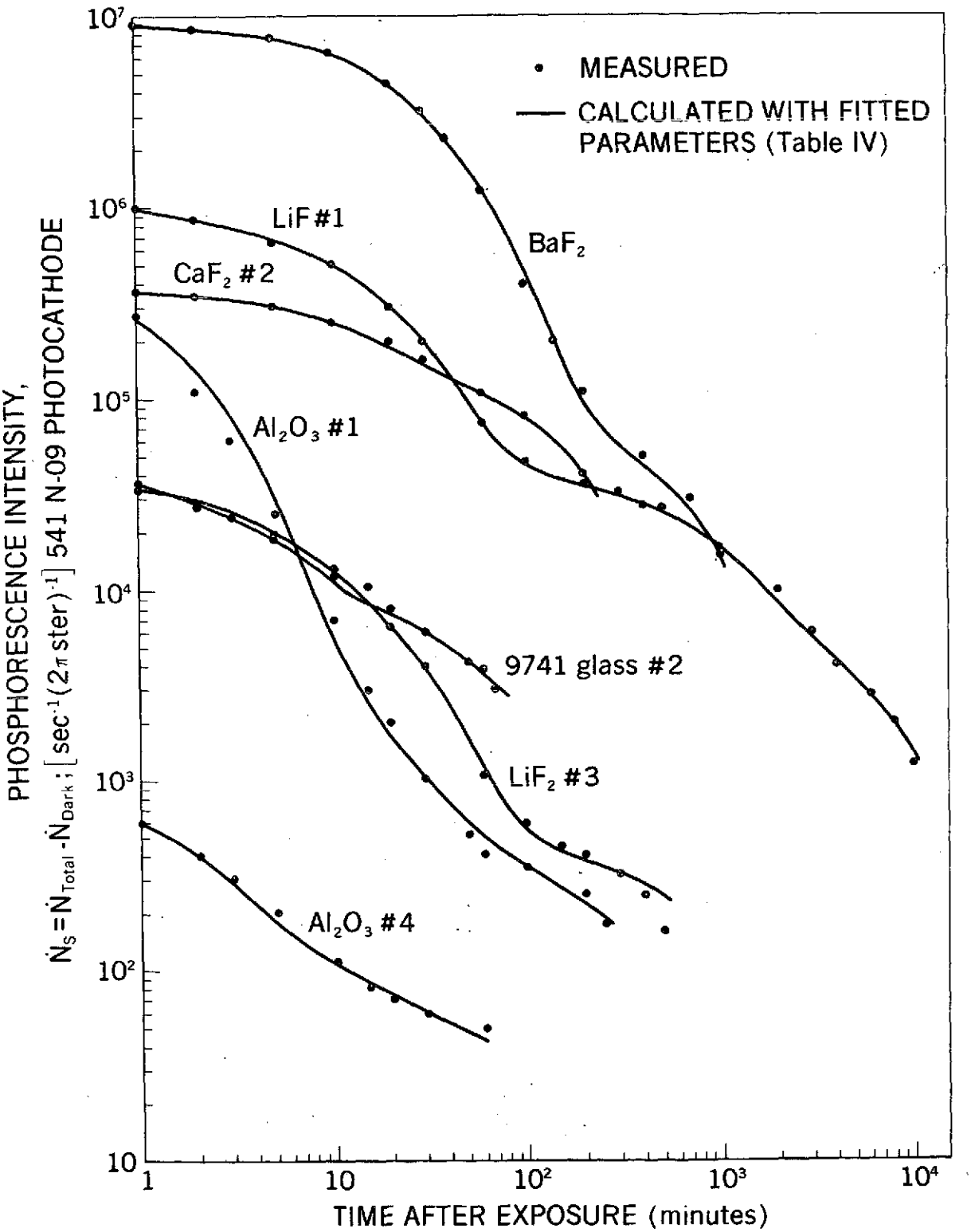
MEASURED
CALCULATED WITH FITTED PARAMETERS (Table IV)
BaF2
LiF #1
CaF2 #2
Al2O3 #1
9741 glass #2
LiF2 #3
Al2O3 #4
PHOSPHORESCENCE INTENSITY, Ṅs = Ṅtotal - Ṅdark ; [sec-1(2π ster)-1] 541 N-09 PHOTOCATHODE
TIME AFTER EXPOSURE (minutes)
10^7
10^6
10^5
10^4
10^3
10^2
10
1
10
10^2
10^3
10^4

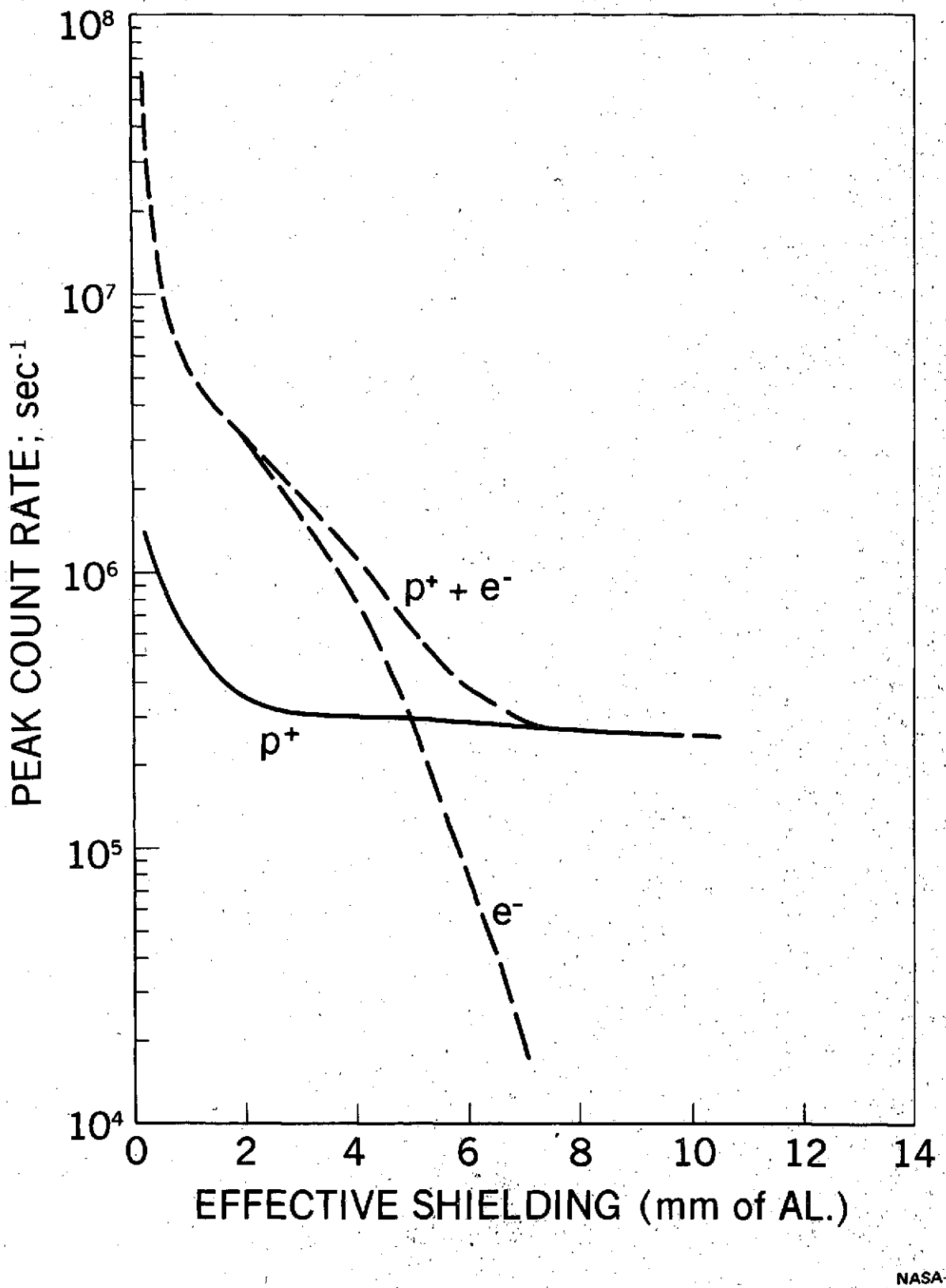
10^8
10^7
10^6
10^5
10^4
PEAK COUNT RATE; sec^{-1}
$p^+ + e^-$
p^+
e^-
0
2
4
6
8
10
12
14
EFFECTIVE SHIELDING (mm of AL.)
NASA–GSFC